Talanta 83 (2011) 1580–1585

Contents lists available at ScienceDirect

Talanta

journal homepage: www.elsevier.com/locate/talanta

A simple double-bead sandwich assay for protein detection in serum using UV–vis spectroscopy

Hilde Jans[a,b,*], Karolien Jans[a], Pieter-Jan Demeyer[a,c], Karel Knez[a,c], Tim Stakenborg[a], Guido Maes[b], Liesbet Lagae[a,d]

[a] imec, SSET/Functional Nanosystems, Kapeldreef 75, B-3001 Leuven, Belgium
[b] KULeuven, Department of Quantum Chemistry and Physical Chemistry, Celestijnenlaan 200F, B-3001 Leuven, Belgium
[c] KULeuven, Department of Biosystems, Division Mechatronics, Biostatistics and Sensors, Willem de Croylaan 42, B-3001 Leuven, Belgium
[d] KULeuven, Department of Solid State Physics and Magnetism, Celestijnenlaan 200D, B-3001 Leuven, Belgium

ARTICLE INFO

Article history:
Received 27 July 2010
Received in revised form 8 November 2010
Accepted 22 November 2010
Available online 30 November 2010

Keywords:
Magnetic nanoparticles
Gold nanoparticles
Immunoassay

ABSTRACT

In this study a double-bead sandwich assay, employing magnetic nanoparticles and gold nanoparticles is proposed. The magnetic nanoparticles allow specific capturing of the analyte in biological samples, while the optical properties of the gold nanoparticles provide the signal transduction. We demonstrated that a major improvement in the assay sensitivity was obtained by selecting an optimal gold nanoparticle size (60 nm). A detection limit of 5–8 ng/mL, a sensitivity of 0.6–0.8 $(pg/mL)^{-1}$ and a dynamic range of 3 orders of magnitude were achieved without any further amplification using the detection of prostate specific antigen in serum as a model system. The proposed assay has the ability to be easily implemented within a microfluidic device for point-of-care applications whereby the readout can be executed by a fast and cheap optical measurement.

1. Introduction

The integration of nanoparticles into lab-on-a-chip devices has the potential to improve point-of-care applications. For example, nanoparticles have been used for the detection of analytes [1,2] and for a combined detection and controlled transport of cells [3], proteins and DNA [4,5]. These, so-called 'bead-based immunoassays' offer several advantages over traditional, two-dimensional technologies. Most importantly, nanoparticles bare a large surface area and the reactions are no longer governed by planar diffusion, but by a faster radial diffusion [6].

Several double-bead assays have already been proposed. For example, metal nanoparticles and more specifically gold nanoparticles (GNPs) have gained considerable attention in the field of biosensing and immunoassay development due to their interesting optical properties and superior biocompatibility [7,8]. Upon illumination, GNPs display a plasmon band around 520 nm in the visible range of the electromagnetic spectrum, which is at the origin of their characteristic red color [9,10]. The sensitivity of the plasmon position towards changes in the local environment of gold nanoshells was applied in the construction of sandwich assays [7]. This simple, low cost technique which can operate in whole blood has one major limitation, i.e. a limited detection limit [7].

On the other hand, GNPs are also phenomenal light scatterers. This characteristic was used in the development of sandwich assays using a combination of GNPs [7,11] and GNPs of different shapes [12], coupled with dynamic light scattering (DLS). These sensitive and easy to perform size measurements, suffer from sample inhomogeneity since proteins can easily form complexes and aggregates. Therefore, the resulting nanoparticle clusters and aggregates induce large measurement-to-measurement variations [13].

Furthermore, combinations of GNPs and quantum dots were used in the development of sensitive inhibition assays [14,15] and indirect assays [16]. The proximity of a GNP near a quantum dot is required to transduce the binding event [7,16], i.e. the quenching or enhancement of the quantum dot's emission. Despite their innovative aspect and high sensitivity, these immunoassays require detailed assay development and suffer from poor general applicability. Moreover, quantum dots are known to be potentially toxic [16].

More interesting towards immunoassay development are magnetic nanoparticles (MNPs) in combination with GNPs. MNPs can be used to isolate and concentrate the target analyte [14,17] and as such alleviate the need for labor-intensive separation steps. Recently, an advanced sandwich assay using MNPs and GNPs encoded with DNA was developed. Polymerase chain reaction allows the detection of proteins in attomolar concentrations [18]. Despite the excellent sensitivity, this strategy requires advanced GNPs functionalization with both DNA and proteins. Moreover, this

* Corresponding author. Tel.: +32 16 287896; fax: +32 16 281097.
E-mail address: Hilde.Jans@imec.be (H. Jans).

0039-9140/$ – see front matter © 2010 Elsevier B.V. All rights reserved.
doi:10.1016/j.talanta.2010.11.057

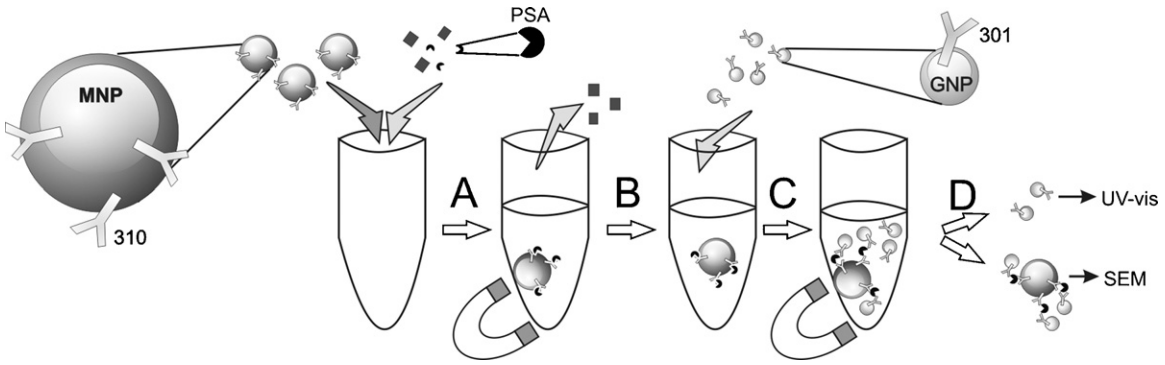

Fig. 1. Schematic representation of the performed double-bead assay. A) MNP-310 were mixed with PSA. B) After incubation, the specific analyte interacted with the MNP-310, and was magnetically separated from the non-specific analyte. C) GNPs-301 were added to the reaction mixture, leading to the capturing of the analyte in a sandwich structure. D) The sandwich structures were magnetically separated from the excess of unbound GNP-301 and investigated using SEM. The supernatant was investigated using UV–vis spectroscopy.

technique needs sophisticated analytical techniques (e.g. PCR) and advanced chip processing to automate the process [2,18].

In the present study, a simple, general, low cost, and easy to automate double bead-based immunoassay has been developed using commercially available MNPs and GNPs. By introducing the proper functionality, the magnetic properties of the MNPs allow easy and selective isolation of the analyte, even in complex matrices such as serum. On the other hand, biofunctionalized GNPs can selectively bind the analyte isolated by the MNPs. Moreover, the bright extinction of GNPs makes them ideal candidates for signal transduction. In the present study, the analyte concentration was easily quantified by determining the amount of GNPs, which is simply related to the plasmon intensity through Beer's law. To the best of our knowledge, this simple approach of signal transduction has not been used before for the development of sensitive immunoassays.

In this study, the detection of prostate specific antigen (PSA), which is a marker for prostate cancer, was chosen to demonstrate the effectiveness of the proposed double-bead assay in both buffer and serum environment. Normally, prostate cancer is suspected if the total PSA level is higher than 10 ng/mL [19]. Sensitive and specific detection of PSA (sub ng/mL) for early prostate cancer detection is of great importance [20], even towards point-of-care applications.

2. Materials and methods

2.1. Materials

GNPs of different sizes (40, 50, 60, 80 and 100 nm) were purchased from BBInternational (Cardiff, UK). 20 nm GNPs were synthesized as described in our previous research [21], according to the method of Turkevich. Trisodium citrate was purchased from Acros (Geel, Belgium). Tetrachloroaurate, acetic acid, 4-(2-hydroxyl-ethyl)-1-piperazineethanesulfonic acid (HEPES), Tween20®, bovine serum albumin (BSA) and all other chemicals were obtained from Sigma–Aldrich (Missouri, USA). Monoclonal IgG type antibodies for the capturing of prostate specific antigen (PSA) in a sandwich approach, i.e. PSA66 (310) [22] and PSA19 (301) [22], were obtained from Fujirobio (PA, USA). PSA (P117) and normal female serum samples were obtained from Scipac (Kent, UK). Carboxyl functionalized magnetic nanoparticles (MNPs) with an average diameter of 300 nm were purchased from Ademtech (carboxyl-adembeads, Pessac, France). 1-Ethyl-3-(3-dimethylaminopropyl)-carbodiimide (EDC) and N-hydroxysuccinimide (NHS) were purchased from BIAcore (GE Healthcare, UK). The used HBS buffer contains 10 mM HEPES, 150 mM NaCl, 0.005% (v/v) Tween20® and 3.4 mM ethylenediaminetetraacetic acid (EDTA). The pH was adjusted to 7.4 using sodium hydroxide. All chemicals and biomolecules were used as received.

2.2. Biofunctionalization of nanoparticles

The covalent biofunctionalization of the MNPs was carried out as described in our previous research [23]. Briefly, 20 μL of MNPs (5 mg/mL, 2.0×10^{11} nanoparticles/mL in H_2O) was suspended in 875 μL of 10 mM acetate pH 5.5. After 10 min of sonication (Branson, Danbury, USA), 25 μL of EDC (0.4 M) and 100 μL of NHS (0.1 M) were added and the suspension was incubated for 8 min on a shaking device (Multireax, Heidolph–Schwabach, Germany). After incubation, the MNPs were magnetically attracted for 3 min in a Magnetight™ separation stand (Remanence of 0.6–0.7 T, Novagen®, Nottingham, UK) and the supernatant was removed. Subsequently, 1 mL of PSA specific antibody-310 (50 μg/mL in 10 mM acetate pH 5.5) was added to the activated MNPs. After 2 h of incubation on a shaking device, the unbound proteins were removed by washing the MNPs 3 times with HBS buffer using magnetic separation. Finally, the MNPs were resuspended in 500 μL HBS. This procedure was performed 7 times in parallel to reduce the variation associated with the immobilization procedure. All 7 MNP-310 suspensions were mixed prior to use.

For the adsorption of IgG 301 onto the GNP, the GNPs suspension (OD = 1) was adjusted with NaOH to pH 10. Afterwards, an excess of IgG 301 (10 μg/mL in HBS) was added. After 1 h of incubation on a shaking device, BSA (520 μg/mL in H_2O) was added. The GNP suspension was centrifuged after an additional 30 min of incubation. Depending on the GNP size, the centrifugation speed was adapted. The supernatant containing the unbound proteins was removed and the pellet of GNPs was resuspended in HBS buffer.

Both the MNP and GNP conjugates were prepared freshly prior to each immunoassay. Each immunoassay was repeated at least twice to determine the reproducibility.

2.3. Double-bead assay using MNPs and GNPs

A dilution series of PSA was prepared (0, 0.02, 0.2, 2, 5, 10 and 20 μg/mL in HBS) and 50 μL of each PSA concentration was added to 450 μL of MNP-310. Each suspension was incubated for exact 1 h (Fig. 1A) at room temperature. The pellets containing MNP-310 bound to PSA (MNP-310/PSA) were separated from the unbound fraction of the sample using magnetic separation. Afterwards the samples were resuspended in 450 μL HBS. Then, 450 μL of GNPs-301 was added to the MNP-310/PSA mixture (Fig. 1B). Exactly after 1 h of incubation, the sandwich complexes were magnetically sep-

Table 1
The experimental position of the plasmon band compared to the theoretical position according to the Mie theory [9]. The GNP concentration at OD 1 was determined [25]. In addition, calculations of the contributions of scattering and adsorption to the total extinction cross-section of GNPs of different sizes at their plasmon band position.

Sample description	λ(LSPR) exp. (nm)	λ(LSPR) theo. (nm)	[GNP] (nanoparticles/mL)	Cext area (m^2)	Csca area (m^2)	Cabs area (m^2)
GNP 20 nm	523	522	7.2×10^{11}	4.31×10^{-16}	3.67×10^{-18}	4.28×10^{-16}
GNP 40 nm	526	526	9.0×10^{10}	3.78×10^{-15}	2.61×10^{-16}	3.55×10^{-15}
GNP 50 nm	530	530	4.5×10^{10}	7.74×10^{-15}	1.04×10^{-15}	6.81×10^{-15}
GNP 60 nm	534	536	2.6×10^{10}	1.39×10^{-14}	3.17×10^{-15}	1.10×10^{-14}
GNP 80 nm	548	549	1.1×10^{10}	3.82×10^{-14}	1.49×10^{-14}	1.89×10^{-14}
GNP 100 nm	574	571	5.7×10^{9}	5.46×10^{-14}	3.73×10^{-14}	2.10×10^{-14}

arated from the unbound fraction of GNP-301 (Fig. 1C). In order to optically examine the complexes, the amount of unbound GNPs-301 was investigated by UV–vis absorption spectroscopy (Fig. 1D). In addition, the sandwich complexes were visualized by SEM. For sample preparation, the sandwich complexes were resuspended in 50 μL HBS.

It should be mentioned that, the concentration of GNPs used in the development of the double-bead sandwich assay is always in excess compared to the concentration of MNPs (final concentration 3.6×10^9 nanoparticles/mL).

2.4. Determination of the detection limit (LOD) of the double-bead assay

To accurately define the LOD and the sensitivity in HBS, a dilution series over a smaller PSA range was prepared (0, 2, 10, 20, 50, 100, 200 ng/mL in HBS). To determine the assay sensitivity and the LOD in female serum, a dilution series was prepared directly in female serum. From each PSA concentration, 250 μL was added to 250 μL of MNP-310 which were first concentrated twice. The LOD was calculated from the dose–response curve using the formula [24]:

$$\mathrm{LOD} = \frac{\left|3N - I\right|}{S}$$

where N is the noise on the absorbance measurement (± 0.001 a.u.), I the intercept with the Y-axis of the linear fit and S is the sensitivity (the slope of the linear fit).

2.5. Determination of the concentration and coverage percentage of GNPs onto MNPs by UV–vis absorption spectroscopy

The absorbance measurements were performed using a Shimadzu UV-2550 spectrophotometer (Kyoto, Japan). Dose–response curves were obtained by plotting the decrease in absorbance of the GNPs-301 (at their LSPR position), for different concentration of PSA, relative to the reference sample (0 ng/mL PSA). This absorbance difference is related to the amount of GNP-301 captured by the sandwich assay. As described before, the concentration can be calculated from the intensity of the plasmon band knowing the size and the extinction coefficient of the GNPs (according to Beer's law) [25]. By dividing the amount of GNPs-301 captured in the sandwich assay by the amount of MNPs-310 present in the solution, the exact amount of GNPs bound per 100 MNPs was calculated. In addition, the percentage of the MNP surface covered with GNPs during the sandwich formation was calculated as the experimental number of GNPs per 100 MNPs divided by the number of GNPs that would theoretically fit on a single MNP.

2.6. Visualization of the sandwich structure by scanning electron microscopy (SEM)

The SEM images were taken using a Philips XL30 FEG instrument operating at an acceleration voltage of 5 kV. The SEM samples were prepared by cleaning a silicon substrate with water and acetone and drying it with N_2. Afterwards, a drop of the suspension was placed on the cleaned silicon substrate and dried in a dust-free environment.

2.7. Modeling the LSPR properties of GNPs by the Mie theory

The wavelength at maximum LSPR, the extinction, scattering and absorption cross-section of the GNPs were calculated using MiePlot v.3.4.12 (Philip Laven, Geneva, Switzerland). All calculations were performed for spherical GNPs in water (5 °C, density: 0.99996382 kg/m^3).

2.8. Determination of the hydrodynamic diameter of the various nanoparticles

To study the biofunctionalization process of the nanoparticles under investigation, their hydrodynamic diameter was measured using a Zetasizer NanoZS equipped with Zetasizer software 6.01 [26]. All sizes reported were based on intensity averages.

3. Results and discussion

3.1. Evaluation of the optical properties and determination of the concentration of GNPs

The synthesized and commercial GNPs were investigated for their optical properties. In Table 1, the position of the plasmon band determined both experimentally and theoretically is listed. The experimentally determined position of the plasmon band corresponds well with the position calculated with the Mie theory. As a remark, the maximum extinction of the GNPs was normalized to 1.0 to enable comparison of their optical properties.

From the results summarized in Table 1 we observe that the concentration decreases as the GNP size increases. A doubling of the nanoparticle size results in a decrease in the concentration of GNPs by a factor 10 [27]. This can be explained by the optical properties of the GNPs, shown in Table 1. The extinction cross-section of a GNP is the sum of its scattering and its absorption cross-section ($c_{ext} = c_{sca} + c_{abs}$) [28]. For relatively small GNPs (10–70 nm), the contribution of c_{abs} to c_{ext} is predominant. On the other hand, c_{sca} becomes more important when the GNP size increases, since larger nanoparticles scatter the light more efficiently [27]. As a result, the c_{ext} increases almost exponentially with the GNP size as shown in Table 1. This implies that upon GNP size increase, at an optical density of 1, less GNPs are needed to be efficiently detected by UV–vis absorption spectroscopy.

In conclusion, the optical properties of both the synthesized and the commercial gold nanoparticles are in agreement with the theoretical predictions. Furthermore, at a constant optical density, the concentration of the GNPs decreases by increasing their size.

3.2. Optimization of the double-bead sandwich assay

3.2.1. Readout of the double-bead sandwich assay

The MNPs were covalently biofunctionalized using EDC and NHS as coupling reagents to link the carboxylic groups of the MNPs with the primary amino groups of the specific PSA antibody (i.e. monoclonal antibody 310). The covalent strategy is preferred because proteins which are only electrostatically bound to the nanoparticle surface are suspected to desorb, especially in protein-rich environments like serum samples [23]. Since the GNPs will not be dispersed in serum samples (Fig. 1) and covalent binding of proteins requires additional chemical functionalization, biofunctionalization via electrostatic interaction was chosen. As such, the monodisperse GNPs of different sizes were biofunctionalized with a specific monoclonal antibody (301) to target PSA relying on a general, highly efficient and easy adsorption strategy which does not affect the biochemical activity of the antibody [17]. The successful biofunctionalization was verified by UV–vis spectroscopy and DLS measurements, showing, respectively, a shift in the plasmon band position to higher wavelengths and an increase in the hydrodynamic diameter, comparable to our previous results [26] (data not shown).

Next, the biofunctionalized MNPs and the GNPs of different sizes were applied in the double-bead assay as schematically shown in Fig. 1. The obtained sandwich structures and the unbound GNP-301 fraction were investigated by UV–vis absorption spectroscopy as shown in Fig. 2.

The absorbance spectrum of the MNP-310 is shown in Fig. 3 at 0 ng/mL PSA. By increasing the concentration of PSA, the spectra of the MNP-310/PSA/GNP-301 complexes exhibit a plasmon band around 557 nm. This band originates from the GNPs-301 and is superimposed onto the absorbance spectrum of the MNPs-310. This indicates the successful formation of sandwich structures (Fig. 1). The absorbance of the GNPs-301 is small compared to the background signal from the MNPs-301. Therefore, this signal cannot be used for a quantitative detection of PSA. Hence, the unbound GNP-301 fraction was investigated. Upon increase of the PSA concentration, more GNPs-301 will be removed from the supernatant due to sandwich formation (MNP-310/PSA/GNP-301). As a consequence, the plasmon band intensity of the GNPs-301 will decrease relative to the amount of PSA added. As such, this strategy allows quantification of the PSA binding event.

In conclusion, the optical readout of the double-bead assay was conducted by an indirect method rather than a direct method. The intensity of the plasmon band of the unbound GNP-301 fraction is more sensitive towards removal of GNPs by sandwich formation (MNP-310/PSA/GNP-301) and is not hampered by the background signal of MNPs. As such, this enables the construction of dose–response curves by plotting the intensity decrease of the plasmon band relative to the PSA concentration.

3.2.2. Influence of the GNP size on the immunoassay

Since the LSPR characteristic of GNPs is dependent on the GNP radius [9,10], the effect of the GNP size on the assay sensitivity was evaluated. Hereto, the double-bead assay was performed using GNP-301 of different sizes (20–100 nm). The corresponding dose–response curves are shown in Fig. 3A. For all six investigated GNP sizes, a saturation level was obtained at a concentration of 500 ng/mL PSA. It is observed that a high saturation signal gives rise to a steep slope of the dose–response curve in the linear region (Fig. 3A). As such, a small change in the PSA concentration will give rise to a large change in the detection signal, resulting in a high sensitivity. Furthermore, it is observed that the smallest (20 nm) and the largest (100 nm) GNPs-301 result in the smallest detection signals at saturation, and the lowest sensitivity (<0.2 pg/mL)$^{-1}$. An optimal detection signal and highest sensitivity was obtained for a

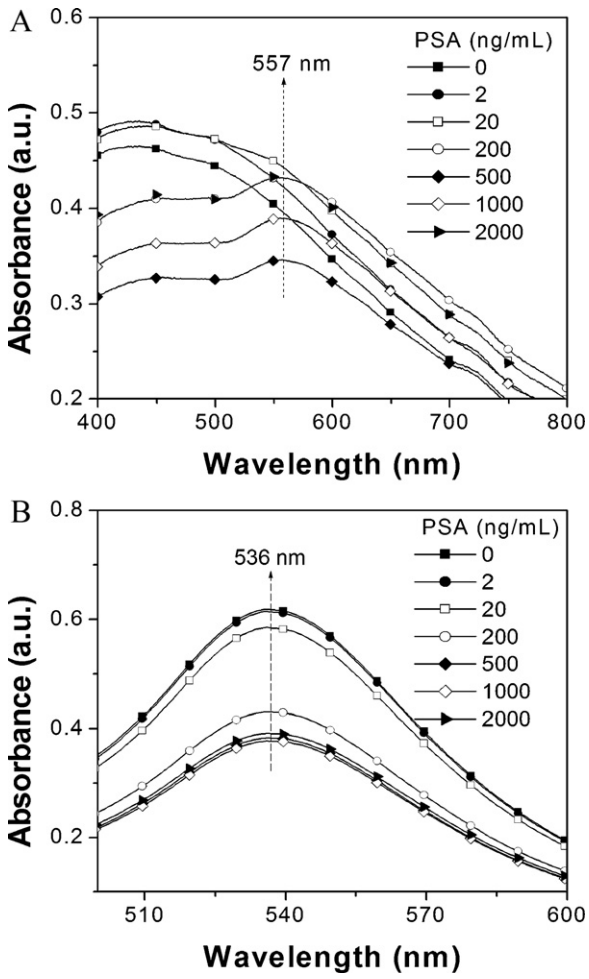

Fig. 2. A) The absorption spectra of the sandwich complexes GNP-301(60 nm)/PSA/MNP-310. By increasing the concentration of PSA, more GNP-301 will bind per MNP-310 leading to an observable plasmon band at 557 nm, superimposed on the background absorption of the MNPs. B) The absorbance spectra of the unbound GNP-301 fraction. Higher PSA concentrations result in lower intensities of the plasmon band located at 536 nm.

GNP size of 60 nm (>0.7 pg/mL)$^{-1}$. The occurrence of this optimum suggests that there are two opposite trends, one favoring large GNPs and the other favoring small GNPs. These two contributions were evaluated into more detail.

First, the total c_{ext} of the GNPs increases almost exponential with the GNP size, as explained previously (Table 1). This implies that the removal of a single, large GNP in the double-bead assay will cause a larger decrease in absorbance compared to the removal of the smaller ones. For this reason, larger particles are would be preferable for use in the double-bead assay. Second, smaller beads have a larger surface-to-volume ratio. An increasing amount of bound GNPs-301 was observed with decreasing GNP size (Fig. 3B). The number of GNPs-301 bound per MNP-310 was also visualized using SEM, as shown in Fig. 3D. Due to their higher electron density, GNPs appear as white dots compared to gray MNPs. The number of GNPs-301 per 100 MNPs-310 at saturation level was roughly estimated from these SEM images (20 nm: 808, 40 nm: 294, 50 nm: 340, 60 nm: 320, 80 nm: 140, 100 nm, 60). The counted values were multiplied by two to account for the fact that only one side of the MNP-310 can be visualized by SEM. The obtained values are comparable to the values calculated from the dose–response curves (Fig. 3B). Additionally, the coverage percentage of GNPs-301 onto the MNP-310 surface was calculated. A linear decrease in the cover-

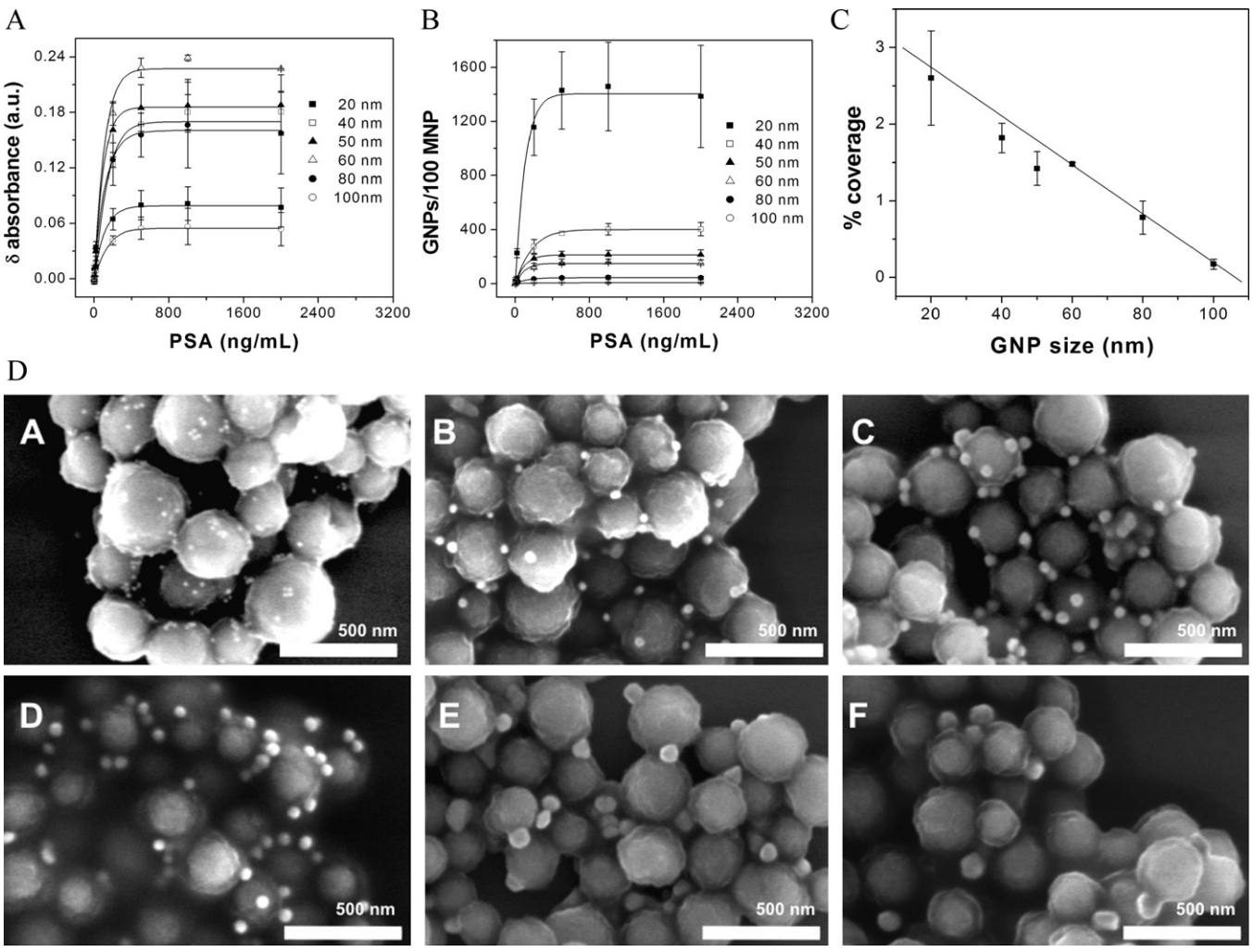

Fig. 3. Dose–response curves for the detection of PSA using different sizes of GNPs. A) The response expressed as a decrease in the plasmon intensity. B) The response as the calculated amount of GNPs per 100 MNPs. C) A plot of the coverage percentage relative to the GNP size. The coverage percentage is determined as the experimental amount of GNPs covering the MNPs (at saturation) relative to the theoretically max amount of GNPs that would fit onto a single MNP. D) SEM image of the sandwich structures obtained by capturing PSA (1 μg/mL) using MNP-310 and GNP-301. The size of the GNPs was varied (A) 20 nm, (B) 40 nm, (C) 50 nm, (D) 60 nm, (E) 80 nm and (F) 100 nm.

age percentage of the MNP-310 surface is observed with increasing GNP size (Fig. 3C).

These findings indicate that small GNPs can form sandwich structures more efficiently. This is supported by the fact that small GNPs are more efficiently biofunctionalized with proteins compared to larger ones, as shown in our previous results [26]. As a remark, a variation in the stabilizing coating (i.e. citrate) of the different GNP sizes might lead to a difference in the biofunctionalization efficiency. However, when evaluating all sizes of GNPs by Fourier Transform Infrared spectroscopy, no difference in the coatings could be observed (data not shown).

Another explanation might be the larger mutual steric hindrance upon sandwich formation with large GNPs, as the coverage percentage decreases with increasing GNP size (Fig. 3C). Potentially, this effect could be more pronounced if the immobilization of anti-PSA antibodies is inhomogenous onto the nanoparticle surface, i.e. assembled in islands.

In conclusion, although the use of large GNPs in the double-bead assay is preferred because of their optical properties, it was shown that large GNPs have worse binding properties compared to smaller ones. These two opposing trends counteract each other and give rise to an optimum in the PSA detection by means of the double-bead sandwich assay using both MNPs and 60 nm GNPs.

3.2.3. Determination of the assay sensitivity and LOD

As concluded in the previous section, performing the double-bead assay with 60 nm GNPs yields the best detection signals. Therefore these GNPs were used to determine the sensitivity and the LOD of the double-bead assay in both buffer and normal female serum. Normal female serum was chosen to avoid small levels of PSA which can be present in male serum. The experimental results are summarized in Fig. 4. It can be observed that there is very limited difference between the performances in buffer and serum except at saturation, where the signals in buffer are slightly higher than in serum (Fig. 4). Since serum samples contain high amounts of proteins (typically from 50–100 mg/mL), non-specific adsorption of these proteins onto the MNPs may slightly block the specific binding sites for PSA and as such decrease the saturation signal. The inserted graph in Fig. 4 represents the calibration graph for the detection of PSA which shows a linear correlation ($R^2 = 0.99$) between the amount of PSA and the absorbance of the unbound fraction of GNPs-301 both in HBS and serum. A LOD of 5–8 ng/mL PSA, a sensitivity of 0.7–0.8 $(pg/mL)^{-1}$ and a dynamic range of three orders of magnitude were obtained using the proposed double-bead assay using 60 nm GNPs. The obtained LOD is lower than the clinically relevant concentration for PSA cancer diagnosis (10 ng/mL [20]), and is competitive with other detection meth-

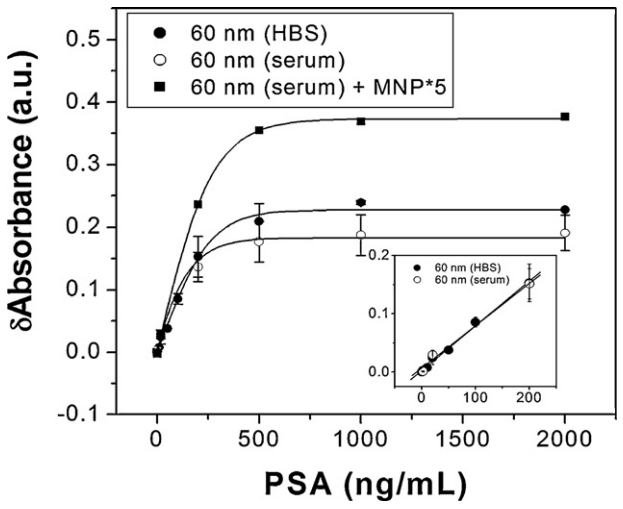

Fig. 4. Dose–response curves for the detection of PSA, performed in buffer and normal female serum. The insert shows the corresponding calibration curves.

ods such as surface plasmon resonance [20] or standard ELISA [19,29].

By surface plasmon resonance, PSA concentrations as low as 10 ng/mL in serum have been directly detected. The LOD was enhanced by using secondary antibodies labeled with gold nanoparticles which allow the detection of 1 ng/mL PSA in serum [20]. For standard ELISA, LODs between 0.5 and 4 ng/mL are frequently reported [19,29]. On the other hand, there are commercially available test on the market which can detect PSA concentration is serum in pg/mL concentrations. However, these high sensitive PSA tests run with automated high-throughput systems, which make them expensive and not appropriate for point-of-care applications [30]. The currently available tests which are well suited for point-of-care applications can measure PSA concentrations as low as 4 ng/mL [30] which is similar to the LOD achieved for the double-bead assay presented in the work.

3.2.4. Influence of the MNPs concentration

As described before, to reach an optimal sensitivity and detection limit with the proposed double-bead assay, 60 nm GNPs were applied in combination with MNPs. To further decrease the detection limit, one can think of increasing the amount of possible sandwich structures (MNP/analyte/GNP). This can be achieved by increasing the amount of MNPs to efficiently isolate the analyte from the serum sample. Hereto, a preliminary study was performed using a fivefold concentration of MNPs. As can be observed from Fig. 4, the saturation signal increases by increasing the MNP concentration. This is expected since more gold nanoparticles can be captured in sandwich structures. It can be observed that the sensitivity, and as such the LOD, can be greatly improved. The latter indicates that by simply increasing the concentration of MNPs, the double-bead assay can reach a lower LOD (sub ng/mL (~pM)) and higher sensitivity. This strongly enhances the potential of the double-bead assay for clinical diagnostics.

4. Conclusions

A simple double-bead assay, using gold and magnetic nanoparticles, was developed for the detection of cancer markers in biological samples. Not all sizes of GNPs were equally suited to perform the double-bead assay. In fact, an optimal detection signal was found for a GNP size of 60 nm. The occurrence of the optimum was ascribed to two counteracting trends. While the Mie theory favors larger GNPs over smaller ones, it was determined by UV–vis spectroscopy and scanning electron microscopy that larger GNPs were functionalized less efficiently with proteins. Furthermore, by using 60 nm GNPs, clinically relevant concentrations for the detection of PSA, a marker for prostate cancer, were obtained. Moreover, the proposed double-bead assay performed equally well in buffer and serum. In addition, by increasing the concentration of MNPs, a further increase in the assay sensitivity and consequently a lower detection limit can be obtained. Although only the detection of PSA was investigated, the method described in this research is believed to be applicable for the detection of other relevant cancer markers since the biofunctionalization of the nanoparticles is very simple and generally applicable. In addition, it is obvious to consider that the proposed 'double-bead' assay can help to elaborate personal diagnostics due to its simplicity and potential use in miniaturized point-of care systems.

Acknowledgement

H. Jans acknowledges the "Institute for the Promotion of Innovation through Science and Technology in Flanders" (IWT-Vlaanderen, H. Jans) for funding. This work was realized within the framework of a research project funded by the EU (Nano3T-214137).

References

[1] P.B. Monaghan, K.M. McCarney, A. Ricketts, R.E. Littleford, F. Docherty, W.E. Smith, D. Graham, J.M. Cooper, Anal. Chem. 79 (2007) 2844–2849.
[2] E.D. Goluch, J.-M. Nam, D.G. Georganopoulou, T.N. Chiesl, K.A. Shaikh, K.S. Ryu, A.E. Barrron, C.A. Mirkin, C. Liu, Lab Chip 6 (2006) 1293–1299.
[3] J.G. Bruno, T. Philips, M.P. Carrillo, R. Crowell, J. Fluoresc. 19 (2009) 427–435.
[4] L.J. Johansson, K. Gunnarsson, S. Bijelovic, K. Eriksson, A. Surpi, E. Göthelid, P. Svedlindh, S. Oscarsson, Lab Chip 10 (2010) 654–661.
[5] S.H. Lim, F. Bestvater, P. Buchy, S. Mardy, A.D.C. Yu, Sensors 9 (2009) 5590–5599.
[6] S.G. Penn, L. He, M.J. Natan, Curr. Opin. Chem. Biol. 7 (2003) 609–615.
[7] L.R. Hirsch, J.B. Jackson, A. Lee, N.J. Halas, J.L. West, Anal. Chem. 75 (2003) 2377–2381.
[8] N.T.K. Thanh, Z. Rosenzweig, Anal. Chem. 74 (2002) 1624–1628.
[9] G. Mie, Ann. Phys. 25 (1908) 377–445.
[10] A.J. Haes, C.L. Haynes, A.D. McFarland, G.C. Schatz, R.P. Van Duyne, S. Zou, MRS Bull. 30 (2005) 368–375.
[11] Q. Dai, X. Liu, J. Coutts, L. Austin, Q. Huo, J. Am. Chem. Soc. 130 (2008) 8138–8139.
[12] X. Lui, Q. Dai, L. Austin, J. Coutts, G. Knowles, J. Zou, Z. Chen, H. Chen, Q. Huo, J. Am. Chem. Soc. 130 (2008) 2780–2782.
[13] Q. Huo, Colloids Surf. B 78 (2010) 259–265.
[14] L. Ao, F. Gao, B. Pan, R. He, D. Cui, Anal. Chem. 78 (2006) 1104–1106.
[15] E. Oh, M.-Y. Hong, D. Lee, S.-H. Nam, H.C. Yoon, H.-S. Kim, J. Am. Chem. Soc. 127 (2005) 3270–3271.
[16] P. Sharma, S. Brown, G. Walter, S. Santra, B. Moudgil, Adv. Colloid Interface Sci. 123 (2006) 471–485.
[17] A. Fan, C. Lau, J. Lu, Anal. Chem. 77 (2005) 3238–3242.
[18] J.-M. Nam, C.S. Thaxton, C.A. Mirkin, Science 301 (2003) 1884–1886.
[19] S. Zhang, P. Du, F. Li, Talanta 72 (2007) 1487–1493.
[20] L. Huang, G. Reekmans, D. Saerens, J.M. Friedt, F. Frederix, L. Francis, S. Muyldermans, A. Campitelli, C. Van Hoof, Biosens. Bioelectron. 21 (2005) 483–490.
[21] H. Jans, T. Stakenborg, K. Jans, B. Van de Broek, S. Peeters, K. Bonroy, L. Lagae, G. Borghs, G. Maes, Nanotechnology 21 (2010) 285608.
[22] O. Nilsson, A. Peter, I. Andersson, K. Nilsson, B. Grundström, B. Karlsson, Br. J. Cancer 75 (1997) 789–797.
[23] H. Jans, K. Jans, T. Stakenborg, B. Van de Broek, L. Lagae, G. Maes, G. Borghs, Impact of pre-concentration to covalently biofunctionalize suspended nanoparticles, Nanotechnology 21 (2010) 345102.
[24] R. De Palma, G. Reekmans, W. Laureyn, G. Borghs, G. Maes, Anal. Chem. 79 (2007) 7540–7548.
[25] X. Liu, M. Awater, J. Wang, Q. Huo, Colloids Surf. B 58 (2007) 3–7.
[26] H. Jans, X. Liu, A. Lauren, G. Maes, Q. Huo, Anal. Chem. 81 (2009) 9425–9432.
[27] N. Nath, A. Chilkoti, Anal. Chem. 76 (2004) 5370–5378.
[28] J. Yguerabide, E.E. Yguerabide, Anal. Biochem. 262 (1998) 157–176.
[29] www.biocompare.com.
[30] D.A. Healy, C.J. Hayes, P. Leonard, L. McKenna, R. O'Kennedy, Trends Biotechnol. 25 (2007) 125–131.